IOP Publishing J. Phys. Mater. 7 (2024) 045004 https://doi.org/10.1088/2515-7639/ad71f5

Journal of Physics: Materials

OPEN ACCESS

RECEIVED
6 May 2024

REVISED
7 August 2024

ACCEPTED FOR PUBLICATION
21 August 2024

PUBLISHED
29 August 2024

PAPER

Electronic transport in reactively sputtered Mn_3GaN films prepared under optimized nitrogen flow

Christoph Sürgers[1,*], **Gerda Fischer**[1], **Sihao Deng**[2,3], **Dongmei Hu**[4] and **Cong Wang**[4,5]

[1] Physikalisches Institut, Karlsruhe Institute of Technology, Kaiserstraße 12, Karlsruhe, D-76131, Germany
[2] Institute of High Energy Physics, Chinese Academy of Sciences, Beijing 100049, People's Republic of China
[3] Spallation Neutron Source Science Center, Dongguan 523803, People's Republic of China
[4] School of Physics, Beihang University, Beijing 100191, People's Republic of China
[5] School of Integrated Circuit Science and Engineering, Beihang University, Beijing 100191, People's Republic of China
[*] Author to whom any correspondence should be addressed.

E-mail: christoph.suergers@kit.edu

Keywords: thin films, antiperovskite, antiferromagnetism, nitride films, reactive sputtering, resistivity, anomalous Hall effect

Abstract

Mn-based nitrides with antiperovskite structures have several properties that can be utilized for antiferromagnetic spintronics. Their magnetic properties depend on the structural quality, composition and doping of the cubic antiperovskite structure. Such nitride thin films are usually produced by reactive physical vapor deposition, where the deposition rate of N can only be controlled by the N_2 gas flow. We show that the tuning of the N content can be optimized using low temperature resistivity measurements, which serve as an indicator of the degree of structural disorder. Several Mn_3GaN_x films were prepared by reactive magnetron sputtering under different N_2 gas flows. Under optimized gas flow conditions, we obtain films that exhibit a metal-like temperature dependence of the resistivity, a vanishing logarithmic increase of the resistivity towards zero, the highest resistivity ratio, and a lattice contraction of 0.4% along the growth direction when heated above the Néel temperature T_N. The retarded formation of an additional magnetic phase appearing at a temperature $T^* \ll T_N$ gives rise to a large thermal hysteresis of the resistivity and anomalous Hall effect.

1. Introduction

Intermetallic compounds with antiperovskite structures provide several interesting physical and chemical properties that can be exploited for technical purposes such as advanced batteries, magnetoresistance, adjustable thermal expansion behavior, and luminescence [1, 2]. In particular, Mn-based antiperovskites Mn_3AX (A = Co, Ni, Zn, Ga, Ge, Ag, Zn; X = N,C) are multifunctional materials with strong magnetostructural and magnetoelastic coupling that give rise to considerable magnetovolume effects, piezomagnetism, enhanced barocaloric response, and giant magnetostriction [1, 3–7]. In Mn_3AX, the Mn atoms in the (111) planes of the cubic structure are arranged in a kagome lattice with antiferromagnetically coupled magnetic moments. The geometrical frustration between the moments leads to coplanar but noncollinear Γ^{4g} or Γ^{5g} magnetic structures with very low magnetization [2, 8–10]. Noncollinear antiferromagnetic order is often the origin of important magnetic properties like the anomalous Hall effect (AHE), spin Hall effect, and spin torque switching that can be utilized in future antiferromagnetic spintronic devices [11–13]. The magnetic configuration strongly affects the AHE, where Γ^{4g} and Γ^{5g} have a finite or zero AHE, respectively [14]. These magnetic antiperovskites are often susceptible to biaxial strain and tetragonal distortions which can lead to the appearance or enhancement of a AHE [15].

However, small variations in stoichiometry can lead to substantial changes of the structural and magnetic properties [16–19]. N deficiency often leads to an increase of the Néel temperature T_N and a broadening of the phase transition observed in the thermal expansion [16, 20]. Usually, structural analysis by x-ray or neutron diffraction is used for tuning and optimizing the alloy composition to obtain the structural or magnetic properties. Recently, detailed structural analysis demonstrated that the displacement of Mn atoms lowers the symmetry of the system, thereby allowing the generation of a nonzero AHE, which would otherwise cancel out in a perfect crystal by spin rotation of different antiferromagnetic domains [21].

While much work has been done on bulk compounds obtained by solid-state reactions at high temperatures, the synthesis of films with reasonable structural order is challenging, particularly when performed in a reactive environment necessary for the preparation of nitride films. In this respect, electrical resistance is a physical property that is easy to measure, albeit often difficult to interpret, and sensitive to the effects of disorder and structural and magnetic phase transitions. It provides a method to optimize the N content to obtain the desired film composition. In this work we have investigated Mn_3GaN_x films obtained by reactive magnetron sputtering in Ar atmosphere under different N_2 flows Φ. Mn_3GaN is an noncollinear antiferromagnet with T_N between 280 and 380 K [10, 17, 20, 22]. $T_N = 300$ K observed for bulk Mn_3GaN is shifted to 380 K by strain in Mn_3GaN/Pt bilayers [23] and electrical current switching of the magnetization has been demonstrated [22]. By analyzing the temperature dependence of the resistivity $\rho(T)$ at low temperatures, we obtain optimized gas flow conditions for synthesis of thin films with minimized structural disorder.

2. Experimental

Substrates were cleaned and heated to 500 °C in a vacuum chamber with a base pressure in the low 10^{-6} mbar range. Films were deposited at 500 °C by dc magnetron sputtering from a single $Mn_{75}Ga_{25}$ alloy target.

Reactive magnetron sputtering is a complex process where the reactive gas reacts at the target, the substrate surface, and at the chamber walls. The stoichiometric and physical properties of the film substantially depend on the type of the reactive gas, the gas flow, and deposition power. The gas flow affects the compound formation of the film due to different deposition modes, i.e. compound formation on the substrate (metal mode) or on the target (poisoned mode), non-linear dependencies of the deposition rate on the flow rate, etc [24, 25]. Due to the number of parameters that influence film growth and compound formation, films reported in this study were deposited always at a total pressure of 10^{-2} mbar, constant dc power of 81 W, constant flow of 40 sccm Ar but with different N_2 gas flows $\Phi = 0$ - 5 sccm. Typical growth rates were 0.03 nm s^{-1}. Deposition rates were calibrated by thickness measurements with a stylus profilometer on thicker samples. Some films were patterned for resistivity measurements by sputtering through a mechanical mask in direct contact with the substrate.

Structural characterization was done by x-ray scattering using a Bruker D8 Discover diffractometer with Cu K_α radiation and the sample temperature was varied by ±20 °C around room temperature by means of a home-built Peltier cooler attached to the sample holder. Measurements of the longitudinal and transverse resistivity were performed in a physical property measurement system (PPMS, Quantum Design). Resistivity measurements were done with a four-point probe on patterned films or in a van der Pauw configuration on planar films. The magnetization was measured in a SQUID magnetometer for magnetic fields up to 5 Tesla applied perpendicular to the film surface.

3. Results and discussion

3.1. Structural characterization

Sputtering without N_2 flow results in the formation of Mn_3Ga with tetragonal structure. Figure 1(a) shows a symmetrical $\theta/2\theta$ x-ray scan of 25 nm Mn_3Ga deposited on MgO (001). The Bragg reflection observed at $2\theta = 51.23°$ corresponds to a lattice plane distance $d = 0.1783$ nm. By comparison with previous studies we assign this peak to the (004) reflection of the tetragonal $D0_{22}$ phase of Mn_3Ga with a lattice constant $c =$ 0.711–0.7133 nm along the growth direction [26–30]. Mn_3Ga is ferrimagnetic with an easy axis along the crystallographic c axis and a high Curie temperature of 730 K [28, 29].

Supplying a flow $\Phi = 0.6$ sccm N_2 results in a change of the x-ray diffraction diagram with a Bragg peak around 46.91°, see figure 1(b) for films deposited on MgO (001) substrates. The variation of the peak intensities from sample to sample is due to the different tilt angles to reduce the strong reflection from the single-crystalline substrate. We identify this peak as the (002) reflection from the cubic Mn_3GaN antiperovskite structure corresponding to a lattice constant $c = 0.3874$ nm along the growth direction in good agreement with bulk Mn_3GaN [31]. The epitaxial growth of the cubic antiperovskite phase is confirmed for $\Phi = 0.6$ sccm by a ϕ-scan of the {311} planes at $2\theta = 82.55°$ ($d = 0.1172$ nm) around the [001] surface normal, see inset figure 1(b). This results in a ratio $c/a = 0.999$ suggesting an almost perfect cubic lattice with negligible tetragonal distortion as reported earlier for a similar low deposition rate of 0.02 nm s^{-1} [18]. Due to the large lattice mismatch of 8% between MgO ($a = 0.4215$ nm) and Mn_3GaN the film is fully relaxed. Increasing the N_2 flow leads to a shift of the (002) peak to lower scattering angles and to a gradual expansion of the Mn_3GaN lattice.

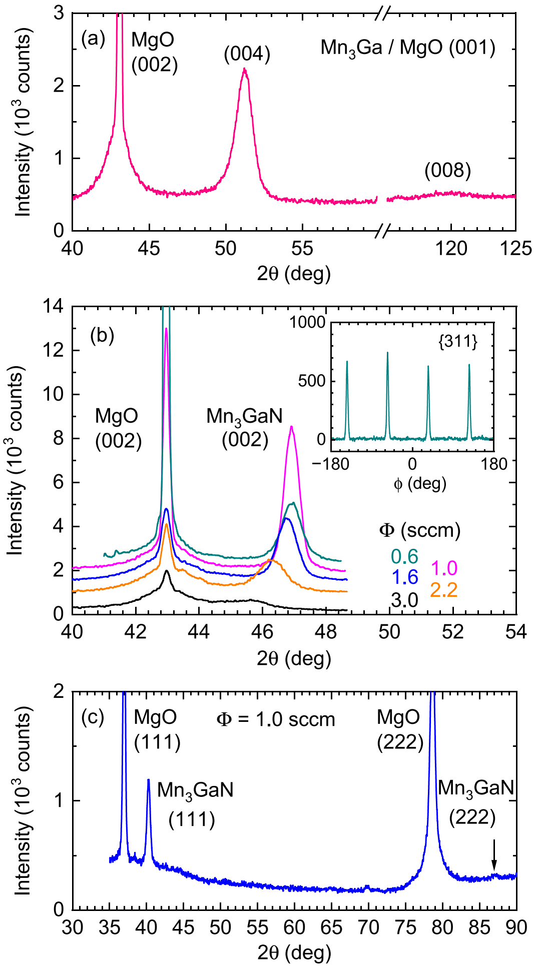

Figure 1. (a) $\theta/2\theta$ x-ray scan of a 25 nm thick Mn_3Ga film on MgO (001). (b) $\theta/2\theta$ x-ray scans of 25 nm thick Mn_3GaN_x films deposited at different N_2 flows Φ on MgO (001). Each sample has been tilted away by 0.5°–1° from the symmetric θ position to reduce the intensity of the strong substrate reflection. Scans have been shifted upward with respect to each other for clarity. Inset shows a ϕ-scan of the $\{311\}$ planes for the film with $\Phi = 0.6$ sccm confirming the fourfold symmetry of the film and substrate. (c) $\theta/2\theta$ x-ray scan of a 25 nm thick Mn_3GaN_x film deposited at $\Phi = 1$ sccm on MgO(111).

On MgO (111), Mn_3GaN grows along the [111] direction with a lattice plane distance $d(111) = 0.2235$ nm corresponding to a lattice constant $c = 0.3871$ nm, similar to the lattice constant for films grown on MgO(001).

3.2. Optimization of nitrogen flow

In the following we focus on the resistivity measurements performed on films prepared under different N_2 gas flows. The temperature dependence of the resistivity ρ, figure 2(a), shows a metallic behavior for all films except for $\Phi = 3.0$ sccm. $\rho(T)$ exhibits a broad and shallow kink around 270 K representing T_N of the antiferromagnetic Γ^{5g} phase [10]. The residual resistivity at low temperatures increases with increasing N_2 gas flow. Note that the film with zero flow represents tetragonal Mn_3Ga with a different structure and should not be compared to the Mn_3GaN_x films. However, a similar metallic-like behavior with a smaller residual resistivity of 30 $\mu\Omega$cm was reported earlier for 240 nm thick films [30].

Except for the film deposited with $\Phi = 1.0$ sccm, $\rho(T)$ in figure 2(b) does not reach a temperature-independent value at low temperatures but instead increases again when cooling to below a temperature T_{min}, where $\rho(T_{\mathrm{min}})$ is considered as the residual resistivity. For $\Phi = 1.0$ sccm (blue squares) we do not observe an increase toward the lowest achievable temperature 1.8 K

The semi-logarithmic plot of $\Delta\rho = \rho(T) - \rho(T_{\mathrm{min}})$ in figure 2(b) clearly shows that $\Delta\rho(T)$ follows a logarithmic temperature dependence $\Delta\rho(T) = \alpha \log(T/T_{\mathrm{min}})$ below T_{min} with a negative slope $\alpha = \mathrm{d}\rho/\mathrm{d}\log(T/T_{\mathrm{min}})$. It is important to note that this logarithmic behavior does not depend on the magnetic field perpendicularly applied to the sample surface, see figure 2(c).

An earlier study on the electronic transport in ferromagnetic $Mn_5Si_3C_x$ films revealed a similar dependence of the low-temperature resisitvity behavior on the carbon concentration [32]. The logarithmic

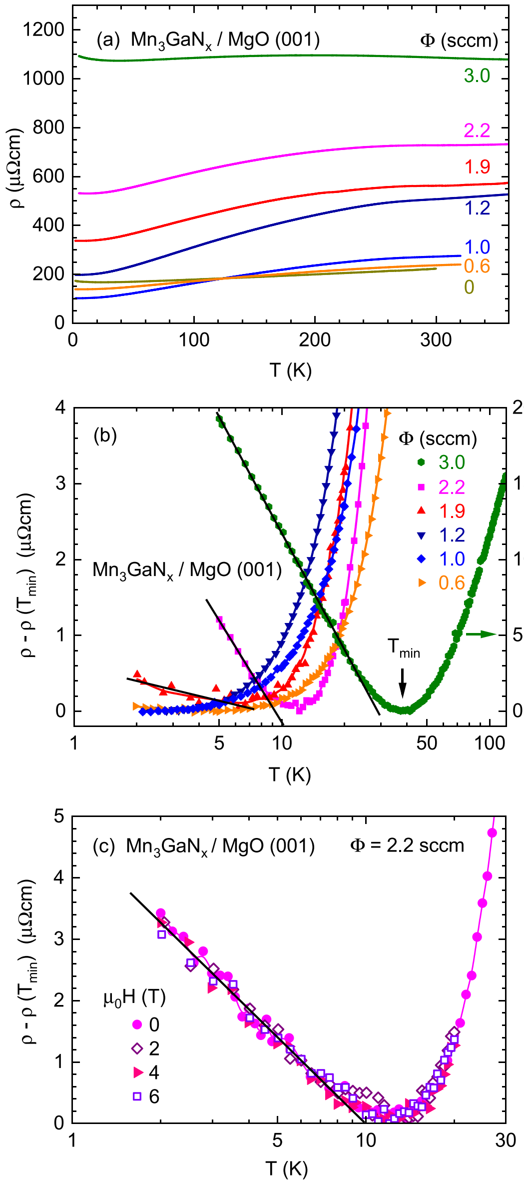

Figure 2. (a) Resistivity ρ vs temperature T of 25 nm thick Mn_3GaN_x films deposited under different N_2 flows Φ on MgO (001) substrates. (b) Semi-logarithmic plot of $\rho - \rho(T_{\min})$, where $T_{\min}$ is the temperature where $\rho(T)$ has a minimum as indicated by the arrow for, e.g. the sample $\Phi = 3.0$ sccm. Solid lines indicate a $\rho \propto \log T$ behavior. (c) $\rho - \rho(T_{\min})$ vs $\log T$ for the film deposited at $\Phi = 2.2$ sccm in different applied magnetic fields H. Solid line indicates a $\rho \propto \log T$ behavior.

increase of the resistivity towards lower temperatures was attributed to the scattering of conduction electrons by structural two-level systems (TLS) [33] and not to other quantum corrections like weak localization or enhanced electron-electron interaction. The latter are expected to change in a magnetic field [34], in contrast to the independence of the logarithmic slope α on an applied magnetic field as large as 6 T shown in figure 2(c).

The behavior can be theoretically described by an orbital Kondo effect that gives rise to a logarithmic $\rho(T)$ dependence around the Kondo temperature T_K [35–38] as experimentally observed in ThAsSe and Ni_xNb_{1-x} metallic glasses [39, 40]. The logarithmic increase of $\rho(T)$ toward low temperatures is due to the increasing coupling between dynamical scatterers and conduction electrons. For further details we refer to [32].

Therefore, we ascribe the logarithmic increase of $\rho(T)$ toward low temperatures of Mn_3GaN_x films to the presence of dynamical scatterers, e.g. atomic vacancies, displaced or interstitial atoms or atoms located in grain boundaries. We use the slope α and the temperature $T_{\min}$ as indicators for the degree of structural disorder. The lower the slope and $T_{\min}$, the higher the structural quality.

The characteristic parameters from x-ray diffraction and electronic transport are summarized in figure 3. Films prepared with $\Phi \approx 1$ sccm are characterized by the lowest residual resistance $\rho_{\min}$, almost zero slope $-\alpha$, and highest residual resistance ratio $\mathrm{RRR} = \rho(300\,\mathrm{K})/\rho_{\min}$. Results obtained on films grown with an optimized gas flow are discussed in the following.

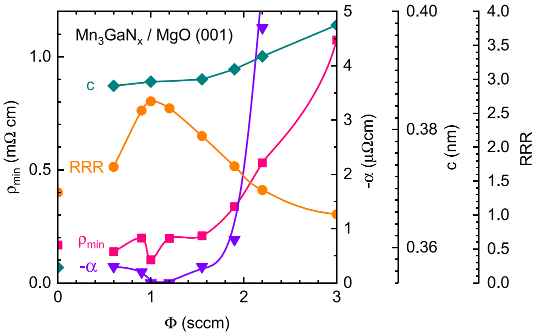

Figure 3. Characteristic parameters of 25 nm thick Mn$_3$GaN$_x$ films on MgO (001) substrates vs N$_2$ flow Φ, see text for details. Solid lines serve as guides to the eye.

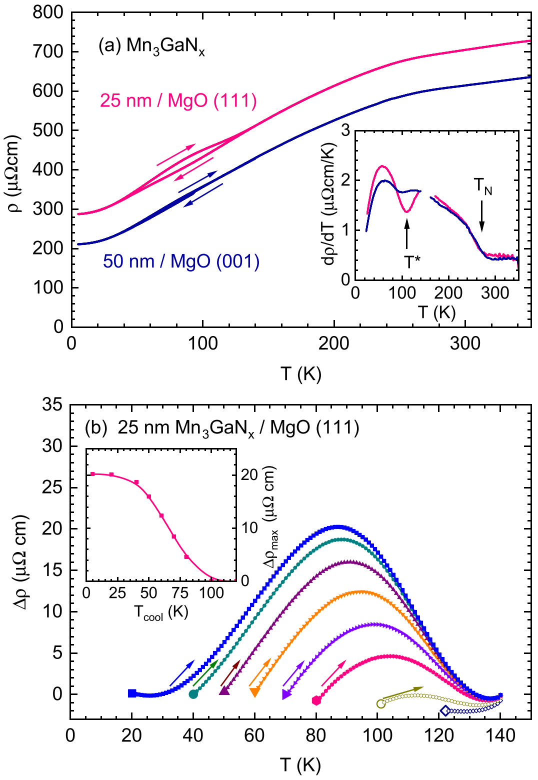

Figure 4. (a) $\rho(T)$ of Mn$_3$GaN$_x$ films on MgO(001) ($\Phi = 1.2$ sccm) and on MgO(111) ($\Phi = 1.0$ sccm) while cooling down and heating up. Inset shows the derivatives $d\rho(T)/dT$ with indicated temperatures T_N and T^*. (b) Resistivity increase $\Delta\rho(T)$ while heating the sample from T_{cool} indicated by large symbols, with respect to the resistivity measured while cooling down from 140 K to T_{cool}. Inset shows the maximum resistivity increase $\Delta\rho_{max}$ vs T_{cool}.

3.3. Coexisting magnetic phase below T^*

The previous data have been obtained while cooling the samples from 350 K down to 2 K. A different temperature dependence was observed when the samples were heated up from 2 K to 350 K. Figure 4(a) shows data of two films prepared under similar conditions on MgO (001) and (111) substrates. For both films, a broad hysteresis of the two datasets appears between 40 K and 140 K, which is stronger for the film deposited on MgO(111). In antiferromagnetic metals, a magnetic phase transition often gives rise to a sudden decrease of the resistivity with an inflexion point representing T_N, corresponding to a local minimum in the derivative $d\rho/dT$ [41]. In the present case, $d\rho/dT$ of the films (inset figure 4(a)) exhibits a broad step at $T_N = 270$ K which we attribute to the Néel temperature of the antiferromagnetic Γ^{5g} phase mentioned before [10, 20]. The resistivity above T_N is only weakly temperature dependent for $T > T_N$ so that only a broad step of $d\rho/dT$ survives at T_N.

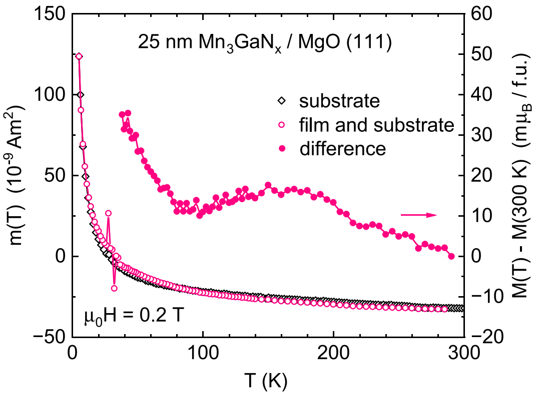

Figure 5. Magnetic moment m (open symbols) and magnetization difference $M - M(300\,\mathrm{K})$ (solid symbols) vs temperature T.

Furthermore, a local minimum appears in $\mathrm{d}\rho/\mathrm{d}T$ at a transition temperature $T^{*} \approx 120\,\mathrm{K}$. The transition at T^{*} was observed previously in $\mathrm{Mn_3GaN}$ films [22, 23] and was assigned to a ferromagnetic-like transition, presumably due to the coexistence of the Γ^{5g} phase and a M-1 phase of tetragonal symmetry and noncollinear and noncoplanar magnetic order. This coexistence was first discovered by neutron powder diffraction analysis below 109 K [5]. The M-1 phase of $\mathrm{Mn_3GaN}$ is particularly interesting because it has been recently suggested as a potential candidate for p-wave magnetic order, where inversion symmetry is broken but the combined translational and time-reversal symmetry is maintained [42]. However, earlier ac susceptibility measurements on $\mathrm{Mn_3GaN}$ indicated the formation of a spin-glass state below a freezing temperature around 133 K [43].

Therefore, we have investigated the thermal hysteresis of $\rho(T)$ of the sample on MgO(111) with the more pronounced hysteresis by performing resistivity measurements with different thermal cycles. Figure 4(b) shows the difference $\Delta\rho(T)$ between the resistivity measured while cooling from 140 K to a temperature T_{cool} and subsequently heating up again to 140 K for various temperatures T_{cool}. $\Delta\rho(T)$ gradually grows with decreasing T_{cool} and reaches a maximum for $T_{\mathrm{cool}} \leqslant 20$ K, see inset figure 4(b). Apparently, the phase transition in the resistivity is fully established only after cooling to temperatures to below 20 K. This suggests that the M-1 phase continuously develops while cooling over a wide temperature range by reformation of the Γ^{5g} phase in agreement with the increasing M-1 phase fraction observed by neutron powder diffraction [5].

The two magnetic phases of $\mathrm{Mn_3GaN}_x$ film are also observed in magnetization measurements. As the magnetization of the thin films is very small, the SQUID magnetometer records strong fluctuations of the signal as soon as the magnetic moment m of the sample (film and substrate) vanishes, see raw data (open circles) around $m(T) \approx 0$ in figure 5. Therefore, we measured m of the bare substrate (black open symbols) and subtracted these data from the raw data. The magnetization $M(T) - M(300\,\mathrm{K})$ of the film on MgO(111) increases continuously with decreasing temperature in the Γ^{5g} phase below 300 K. Below ≈ 100 K, we observe a steeper rise of the magnetization toward lower temperatures which we attribute to the additional contribution from the M-1 phase below T^{*}. An increase of 30 $\mathrm{m}\mu_B$/f.u. corresponds to 0.01 μ_B/Mn, much smaller than 0.2 μ_B/Mn and 0.08 μ_B/Mn previously reported for bulk and thin film $\mathrm{Mn_3GaN}$, respectively, which is presumably due to the smaller M-1 phase fraction in the present case [5, 23].

In the two-phase region below $T^{*} \approx 120$ K we observe an AHE, see figure 6, where the insets show the saturation value at $\mu_0 H = 2$ T. Because of the small AHE for the 50 nm film (figure 6(a)) we subtracted the linear-in-field contribution $\rho^{0}_{yx} = R_{\mathrm{H}}\mu_0 H$ arising from the ordinary Hall effect and obtain $\rho^{\mathrm{A}}_{yx} = \rho_{yx} - \rho^{0}_{yx} = 0.036\,\mu\Omega\mathrm{cm}$ and $R_{\mathrm{H}} = 0.9 \times 10^{-4}\mathrm{cm^3/As}$ at 50 K. The temperature below which the AHE emerges agrees with the transition temperature T^{*} determined from the $\rho(T)$ behavior, figure 4. Similar to the temperature dependence of $\rho(T)$ (figure 4) we observe a strong thermal hysteresis of $\rho_{yx}(2\ \mathrm{T})$ between cooling down and heating up the sample, see inset figure 6(b). Below 40 K both data sets merge in agreement with the saturation of $\Delta\rho_{\max}$ in figure 4(b). The occurrence of a AHE below T^{*} confirms that the phase transition at T^{*} is of magnetic origin, possibly coupled to a change of the crystalline structure. However, the fact that the AHE does not vanish in the M-1 phase below T^{*} requires additional tilting or disordering of the magnetic moments to break the combined translational and time-reversal symmetry that would otherwise prevent an AHE in the perfectly ordered M-1 phase.

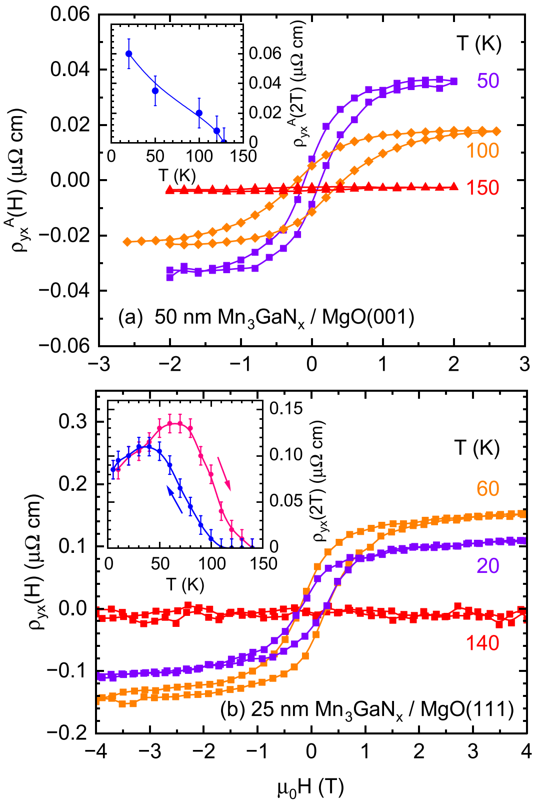

Figure 6. Hall resistivity ρ_{yx} vs applied magnetic field H at different temperatures T for Mn_3GaN_x films on (a) MgO(001) and on (b) MgO(111). Insets show the AHE at $\mu_0 H = 2$ T vs temperature.

For $T >$ 120 K, only the comparatively small ordinary Hall effect appears. This is in line with the fact that for cubic and structurally relaxed antiperovskite Mn_3GaN with Γ^{5g} magnetic structure no AHE is expected [14, 15].

Finally, we mention that for the ferrimagnetic Mn_3Ga film ($\Phi = 0$) we observe an AHE with a broad hysteresis and a coercivity $\mu_0 H_c \approx 2$ T that barely shrinks between 50 K and 300 K due to the high $T_C = 730$ K [28, 29], similar to results previously reported for 240 nm thick films on Mg (001) substrates [30].

3.4. Lattice distortion at T_N

Mn_3GaN is known to exhibit a distortion of the cubic lattice by 0.4% when the temperature changes across T_N [20, 31, 44]. For resolving this lattice distortion in the Mn_3GaN_x films we performed x-ray diffraction at various temperatures close to T_N.

Figures 7(a) and (b) show the (002) and (111) Bragg reflections of Mn_3GaN for films deposited on MgO(001) and amorphous SiO_2, respectively. In both cases, the Bragg reflections shift to higher diffraction angles with increasing temperature corresponding to a decrease of the lattice parameter along the surface normal. From the temperature dependence of the lattice parameters $d(002)$ and $d(111)$, figure 7(c), a strong compression of the crystalline lattice along the surface normal is observed between 275 K and 300 K. We attribute this compression to the transition from the antiferromagnetic Γ^{5g} phase to the paramagnetic phase above T_N and the strong coupling between the crystalline lattice and the magnetic order. Note that this temperature dependence is opposite to what is expected from the usually observed thermal expansion for solid materials. We mention that similar results have been obtained for Mn_3GaN_x films deposited under optimized conditions on other substrates like Si (100) and diamond. For the film on SiO_2, a compression of $\geqslant 0.4\%$ similar to the result for bulk Mn_3GaN is observed. The apparently smaller compression of 0.1% for the film on MgO(001) is due to the slightly reduced transition temperature T_N and the inaccessibility of lower temperatures in the experimental setup in ambient air.

The structural phase transition accompanied with the magnetic phase transition is also observed as a pronounced step in $\rho(T)$ for the thickest film deposited on SiO_2, figure 7(d), with a thermal hysteresis of similar magnitude as observed for the lattice distortion, figure 7(c). We did not observe a clear dependence

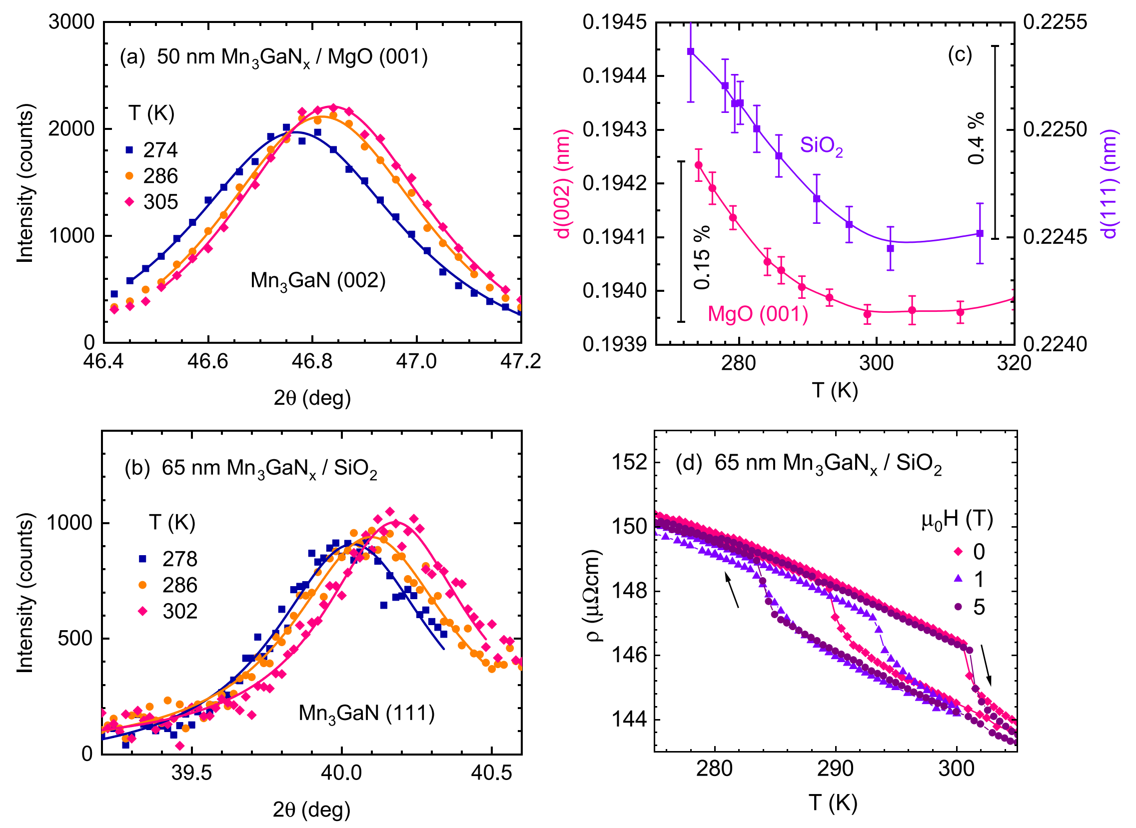

Figure 7. $\theta/2\theta$ x-ray scans of Mn_3GaN_x films on (a) MgO(001) and (b) SiO_2 substrates at different temperatures T. (c) Lattice parameters d determined from the (002) and (111) Bragg reflections vs temperature. (d) Resistivity $\rho(T)$ near the phase transition at T_N for different applied magnetic fields H.

on the applied magnetic field except that the transition takes place at different temperatures in subsequent thermal cycles possibly due to supercooling/superheating effects in a regime of metastable states.

4. Conclusion

Mn_3GaN_x films of antiperovskite structure were grown by reactive dc magnetron sputtering. The detailed study of the resistivity of films prepared under different N_2 gas fluxes Φ shows that the N content can be optimized to obtain films with the required magnetic and structural phase transitions by relying on parameters such as resistivity, the residual resistivity ratio and, in particular, a vanishing increase in resistivity toward low temperatures. In the present case, a N_2 flow $\Phi \approx 1$ sccm has been found to be beneficial for obtaining Mn_3GaN_x films with minimized structural disorder. We propose that this path can be followed in search for optimal conditions for the growth of other antiperovskite nitrides. For films grown under an optimized N_2 gas flow, a broad thermal hysteresis in the resisitivity and AHE below a temperature T^* is observed, indicating a retarded formation of the magnetic M-1 phase.

Data availability statement

The data that support the findings of this study are openly available at the following URL/DOI: https://doi.org/10.35097/gq6y1xwnj6cf6dqk.

Acknowledgments

This work was supported by the Sino-German Mobility Programme No. M-0273.

Conflict of interest

The authors declare no competing interests.

ORCID iDs

Christoph Sürgers https://orcid.org/0000-0002-2132-9775
Gerda Fischer https://orcid.org/0000-0002-7545-1995
Sihao Deng https://orcid.org/0000-0002-5142-3519
Dongmei Hu https://orcid.org/0009-0002-6496-7053
Cong Wang https://orcid.org/0000-0002-4100-4222

References

[1] Wang Y, Zhang H, Zhu J, Lü X, Li S, Zou R and Zhao Y 2020 Antiperovskites with exceptional functionalities *Adv. Mater.* **32** 1905007
[2] Coey J M D, Givord D and Fruchart D 2022 Metallic nitride and carbide perovskites: history and prospects *ECS J. Solid State Sci. Technol.* **11** 055002
[3] Singh H K, Samathrakis I, Fortunato N M, Zemen J, Shen C, Gutfleisch O and Zhang H 2021 Multifunctional antiperovskites driven by strong magnetostructural coupling *npj Comput. Mater.* **7** 1
[4] Takenaka K, Ichigo M, Hamada T, Ozawa A, Shibayama T, Inagaki T and Asano K 2014 Magnetovolume effects in manganese nitrides with antiperovskite structure *Sci. Technol. Adv. Mater.* **15** 015009
[5] Shi K *et al* 2016 Baromagnetic effect in antiperovskite $Mn_3Ga_{0.95}N_{0.94}$ by neutron powder diffraction analysis *Adv. Mater.* **28** 3761
[6] Zemen J, Gercsi Z and Sandeman K G 2017 Piezomagnetism as a counterpart of the magnetovolume effect in magnetically frustrated Mn-based antiperovskite nitrides *Phys. Rev.* B **96** 024451
[7] Lukashev P, Sabirianov R F and Belashchenko K 2008 Theory of the piezomagnetic effect in Mn-based antiperovskites *Phys. Rev.* B **78** 184414
[8] Mochizuki M, Kobayashi M, Okabe R and Yamamoto D 2018 Spin model for nontrivial types of magnetic order in inverse-perovskite antiferromagnets *Phys. Rev.* B **97** 060401
[9] Gomonay O 2015 Berry-phase effects and electronic dynamics in a noncollinear antiferromagnetic texture *Phys. Rev.* B **91** 144421
[10] Fruchart D and Bertaut E F 1978 Magnetic studies of the metallic perovskite-type compounds of manganese *J. Phys. Soc. Japan* **44** 781
[11] Chen H, Liu L, Zhou X, Meng Z, Wang X, Duan Z, Zhao G, Yan H, Qin P and Liu Z 2024 Emerging antiferromagnets for spintronics *Adv. Mater.* **36** 2310379
[12] Baltz V, Manchon A, Tsoi M, Moriyama T, Ono T and Tserkovnyak Y 2018 Antiferromagnetic spintronics *Rev. Mod. Phys.* **90** 015005
[13] Jungwirth T, Marti X, Wadley P and Wunderlich J 2016 Antiferromagnetic spintronics *Nat. Nanotechnol.* **11** 231
[14] Gurung G, Shao D-F, Paudel T R and Tsymbal E Y 2019 Anomalous Hall conductivity of noncollinear magnetic antiperovskites *Phys. Rev. Mater.* **3** 044409
[15] Samathrakis I and Zhang H 2020 Tailoring the anomalous Hall effect in the noncollinear antiperovskite Mn_3GaN *Phys. Rev.* B **101** 214423
[16] Takenaka K, Sugiura T, Kadowaki Y, Ozeki M, Okamoto Y and Fujita A 2021 Giant magneto-volume and magneto-caloric effects of frustrated antiferromagnet Mn_3GaN under hydrostatic pressure *J. Phys. Soc. Japan* **90** 044601
[17] Feng W J, Li D, Deng Y F, Zhang Q, Zhang H H and Zhang Z D 2010 Magnetic and transport properties of Mn_{3+x} Ga_{1-x} N compounds *J. Mater. Sci.* **45** 2770
[18] Ishino S, So J, Goto H, Hajiri T and Asano H 2017 Preparation and evaluation of $Mn_3GaN_{1\text{-}x}$ thin films with controlled N compositions *AIP Adv.* **8** 056312
[19] Han H, Sun Y, Shi K, Yuan X, Ren J, Cui J, Hu D, Zhang K and Wang C 2022 Sign reversal of the anomalous Hall effect in antiperovskite (110)-oriented $Mn_{3.19}Ga_{0.81}N_{1\text{-}d}$ film *J. Appl. Phys.* **132** 233902
[20] Kasugai D, Ozawa A, Inagaki T and Takenaka K 2012 Effects of nitrogen deficiency on the magnetostructural properties of antiperovskite manganese nitrides *J. Appl. Phys.* **111** 07E314
[21] Rimmler B H *et al* 2023 Atomic displacements enabling the observation of the anomalous hall effect in a non-collinear antiferromagnet *Adv. Mater.* **35** 2209616
[22] Hajiri T, Ishino S, Matsuura K and Asano H 2019 Electrical current switching of the noncollinear antiferromagnet Mn_3GaN *Appl. Phys. Lett.* **115** 052403
[23] Hajiri T, Matsuura K, Sonoda K, Tanaka E, Ueda K and Asano H 2021 Spin-orbit-torque switching of noncollinear antiferromagnetic antiperovskite manganese nitride *Phys. Rev. Appl.* **16** 024003
[24] Gudmundsson J T 2020 Physics and technology of magnetron sputtering discharges *Plasma Sources Sci. Technol.* **29** 113001
[25] Azevedo Neto N F, Leite D M G, Lisboa-Filho P N and da Silva J H D 2018 Role of the reactive sputtering deposition power in the phase control of cobalt oxide films *J. Vac. Sci. Technol.* A **36** 061512
[26] Krén E and Kádár G 1970 Neutron diffraction study of Mn_3Ga *Solid State Commun.* **8** 1653
[27] Niida H, Hori T and Nakagawa Y 1983 Magnetic properties and crystal distortion of hexagonal Mn_3Ga *J. Phys. Soc. Japan* **52** 1512
[28] Balke B, Fecher G H, Winterlik J and Felser C 2007 Mn_3Ga, a compensated ferrimagnet with high Curie temperature and low magnetic moment for spin torque transfer applications *Appl. Phys. Lett.* **90** 152504
[29] Kurt H, Rode K, Venkatesan M, Stamenov P and Coey J M D 2011 High spin polarization in epitaxial films of ferrimagnetic Mn_3Ga *Phys. Rev.* B **83** 020405
[30] Bang H-W, Yoo W, Kim C, Lee S, Gu J, Park Y, Lee K and Jung M-H 2019 Structural, magnetic and electrical properties of collinear antiferromagnetic heteroepitaxy cubic Mn_3Ga thin films *Appl. Phys. Lett.* **115** 012402
[31] Takenaka K, Inagaki T and Takagi H 2009 Conversion of magnetic structure by slight dopants in geometrically frustrated antiperovskite Mn_3GaN *Appl. Phys. Lett.* **95** 132508
[32] Gopalakrishnan B, Sürgers C, Montbrun R, Singh A, Uhlarz M and Löhneysen H V 2008 Electronic transport in magnetically ordered Mn_5Si_3 films *Phys. Rev.* B **77** 104414
[33] Cochrane R W, Harris R, Ström-Olson J O and Zuckermann M J 1975 Structural manifestations in amorphous alloys: resistance minima *Phys. Rev. Lett.* **35** 676
[34] Lee P A and Ramakrishnan T V 1985 Disordered electronic systems *Rev. Mod. Phys.* **57** 287
[35] Zawadowski A 1980 Kondo-like state in a simple model for metallic glasses *Phys. Rev. Lett.* **45** 211

[36] Vladár K and Zawadowski A 1983 Theory of the interaction between electrons and the two-level system in amorphous metals. III. Experimentally observable quantities *Phys. Rev.* B **28** 1596

[37] Cox D L and Zawadowski A 1998 Exotic Kondo effects in metals: magnetic ions in a crystalline electric field and tunnelling centres *Adv. Phys.* **47** 599

[38] von Delft J, Ralph D C, Buhrman R A, Upadhyay S K, Louie R N, Ludwig A W W and Ambegaokar V 1998 The 2-channel Kondo model: I. Review of experimental evidence for its realization in metal nanoconstrictions *Ann. Phys., NY* **263** 1

[39] Cichorek T, Sanchez A, Gegenwart P, Weickert F, Wojakowski A, Henkie Z, Auffermann G, Paschen S, Kniep R and Steglich F 2005 Two-channel Kondo effect in glasslike ThAsSe *Phys. Rev. Lett.* **94** 236603

[40] Halbritter A, Kolesnychenko O Y, Mihály G, Shklyarevskii O I and van Kempen H 2000 Transport properties and point-contact spectra of Ni_xNb_{1-x} metallic glasses *Phys. Rev.* B **61** 5846

[41] Alexander S, Helman J S and Balberg I 1976 Critical behavior of the electrical resistivity in magnetic systems *Phys. Rev.* B **13** 304

[42] Hellenes A B, Jungwirth T, Sinova J and Šmejkal L 2023 Unconventional p-wave magnets (arXiv:2309.01607)

[43] Song B, Jian J, Bao H, Lei M, Li H, Wang G, Xu Y and Chen X 2008 Observation of spin-glass behavior in antiperovskite Mn_3GaN *Appl. Phys. Lett.* **92** 192511

[44] Nan T *et al* 2020 Controlling spin current polarization through non-collinear antiferromagnetism *Nat. Commun.* **11** 4671